JOURNAL OF MAGNETIC RESONANCE 78, 133–141 (1988)

EPR Spectra of Quintet Ferrous Myoglobin and a Model Heme Compound

MICHAEL P. HENDRICH* AND PETER G. DEBRUNNER

Department of Physics, University of Illinois, 1110 West Green Street, Urbana, Illinois 61801

Received August 3, 1987; revised October 29, 1987

We report observations and analyses of low-temperature Fe(II) EPR signals in frozen solutions of myoglobin (Mb), the spin $S = 2$ O_2-storage protein of mammals. Of interest is a better understanding of the magnetic properties of the biologically active states from quintet EPR signals we recently discovered (*1*). The salient properties of the EPR spectra are weak intensity; broad, low-field valley in dx''/dB near 100 mT; finite χ'' at $B = 0$; observation below 30 K only; and field-dependent saturation. We also report EPR and magnetic susceptibility results on related octahedrally coordinated ferrous compounds.

It is generally assumed that high-spin ferrous myoglobin complexes are EPR silent at X band. Since ferrous complexes are non-Kramers systems, they have no degeneracies in low symmetry for $B = 0$ that would lead to energy splittings $\Delta E = h\nu$ when the appropriate magnetic field is applied. Therefore, in comparison to the vast literature on ferric myoglobin, there are little direct EPR data on the biologically active ferrous complexes.

Much is known about the structure of the Mb active center and its magnetic properties. Therefore, it is important to check the compatibility of the new EPR spectra with the current models. The quintet state is usually parametrized in terms of the spin Hamiltonian (*2*)

$$\mathscr{H} = D(S_z^2 - 2) + E(S_x^2 - S_y^2) + \beta \mathbf{B} \cdot \mathbf{g} \cdot \mathbf{S}, \qquad |E/D| \leqslant 1/3. \qquad [1]$$

Figure 1 shows an energy level diagram and results from perturbation theory, for the case $D \gg E, g_{zz}\beta B$. In the compounds of interest D is large, and $\Delta m_s = \pm 1$ transitions are observable only in the far infrared (*3–5*). However, the two "non-Kramers doublets" in Fig. 1 may have energy splittings ΔE sufficiently small to satisfy the resonance condition $\Delta E = h\nu \approx 0.3$ cm^{-1} at X band (9 GHz). For these non-Kramers doublets, $|\pm'\rangle$, we have $\langle +'|S_\pm|-'\rangle = 0$, but for $E \neq 0$, $\langle +'|S_z|-'\rangle \neq 0$; thus a component of the microwave field along the z axis of the g tensor will stimulate transitions. To accommodate this selection rule we use a special microwave cavity.

The splitting of these non-Kramers doublets depends on the parameters D and E. Evidence presented here and in other work (*4, 6, 7*) strongly suggests wide distributions

* Present address: Freshwater Biological Institute, University of Minnesota, PO Box 100, Navarre, Minnesota 55392.

0022-2364/88 $3.00

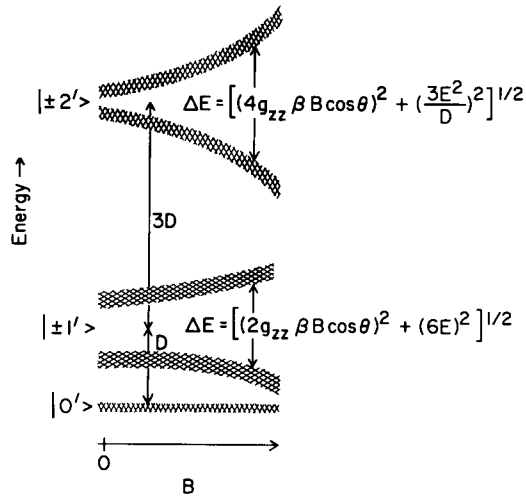

FIG. 1. Energy level diagram of a quintet ($S = 2$) state with energy splittings ΔE of the non-Kramers doublets for the case $D \gg E$, $g_{zz}\beta B$, and $D > 0$. States $|0'\rangle$, $|\pm 1'\rangle$, and $|\pm 2'\rangle$ are eigenfunctions of Eq. [1]. For $B = 0$, $|0'\rangle$ and $|\pm 2'\rangle$ are linear combinations of the $m_s = 0, \pm 2$ states, while $|\pm 1'\rangle$ are linear combinations of the $m_s = \pm 1$ states. The angle between **B** and the z axis of Eq. [1] is θ.

in these parameters, reflecting structural variations in frozen protein solutions. This is indicated in Fig. 1 by a width of the energy levels. We also present contrasting data on a crystal sample with a small width in the zero-field parameter distribution. In order to extract quantitative information, we have developed a spectral simulation program, which assumes distributions in D and E. Eventually, such information in D and E will be related to more fundamental quantities, e.g., orbital energy level splittings. Starting with Bleaney's (*2, 8*) perturbation analysis for $D \gg E$, $g_{zz}\beta B$, simulations of reasonable quality are obtained. However, all simulations in this report use full matrix diagonalization and the extension to higher frequencies is thus straightforward. Note that Bleaney's as well as Hagen's (*7*) treatment lacks the factor $dB/d\nu$ required for field-swept spectra (*9*).

Our simulation program assumes a delta function for the spin packet lineshape, and a Gaussian distribution for D and E. Discrete arrays in erf(D), erf(E), and cos θ are created, which contain information on the resonant magnetic field and transition probability. The g values for each diagonalization point are determined to second order in spin–orbit coupling using the relations (*10*)

$$\begin{aligned} g_{yy} &= g_{zz} - (2k/\lambda)(D + E) \\ g_{xx} &= g_{zz} - (2k/\lambda)(D - E) \\ g_{zz} &= 2 \qquad\qquad (D > 0) \\ g_{zz} &\geqslant 2 + (2k/\lambda)(|D| + |E|) \qquad (D < 0), \end{aligned} \tag{2}$$

where $\lambda = 100$ cm^{-1}, $k = 0.8$ for heme iron, and $k = 1$ for hexaquo iron(II). The resonance field array is contoured in discrete intervals ΔB. The area of each contour,

multiplied by appropriate intensity factors, is added into the bin for that magnetic field to create a spectrum.

EPR measurements were taken on a Bruker 200D X band (9 GHz) spectrometer using an Oxford liquid helium flow cryostat. A bimodal Varian E-236 microwave cavity was used to generate a mode pattern with $B_1 \parallel B$. This mode enhances S/N twofold and attenuates ferric impurity signals by ~200. Also, by a simple change in the microwave frequency, a standard $B_1 \perp B$ mode can be generated. Temperature measurement was accomplished using the EPR signal of metmyoglobin, $D/k = 13.7$ K (*11*). Metmyoglobin was either an impurity or purposely introduced by placing it in a capillary and freezing it into the sample. The usual thermometry method employed by commercial instruments for EPR does not give reliable information near liquid helium temperatures.

For comparison with other $S = 2$ ferrous states, we report results on two hexaquo Fe(II) "standards": zinc fluosilicate with 4% iron doping [(Zn/Fe)FS] and a frozen aqueous ferrous sulfate solution. The magnetic properties of (Zn/Fe)FS with various amounts of iron have been analyzed previously with EPR (*12*), far-infrared (*3, 5*), pulsed magnetic field (*13*), and Mössbauer (*14*) spectroscopies. Figure 2a shows derivative EPR spectra of a single crystal of (Zn/Fe)FS as a function of angle. The finite value of χ'' at $B = 0$, as shown in Figs. 2b and 2c, indicates that only a fraction of all

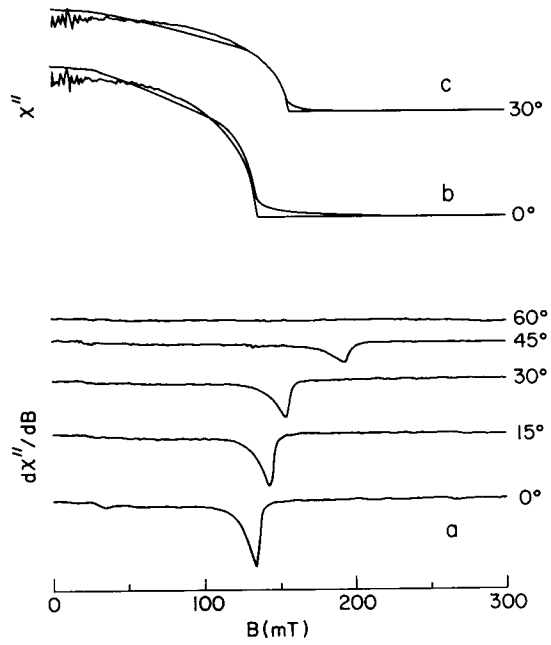

FIG. 2 Single crystal EPR spectra and simulations of 4% iron-doped zinc fluosilicate [(Zn/Fe)FS] at $T \approx 15$ K using $B_1 \parallel B$. (a) Rotation, $0° < \alpha < 60°$, about an axis perpendicular to the trigonal [1, 1, 1] distortion axis, where α is the angle between **B** and the [1, 1, 1] axis. Approximate number of spins is 10^{16}. Simulations of χ'' at (b) 0° and (c) 30° use $E_0/k = 0.06$ K, $\sigma_E/k = 0.06$ K, $\mathbf{g} = (2.26, 2.26, 2.40)$ (*12*). Instrumental parameters: microwave, 9.107 GHz at 2 mW; modulation, 100 kHz at 0.8 mT_{pp}; gain, 2×10^5; field sweep, 1.5 mT/s. Noise at $B = 0$ in the simulation is dependent on the number of integration points.

the molecules have a suitable pair of energy levels (zero-field splitting less than $h\nu$) that can give rise to EPR transitions at X band. At Q band (35 GHz), we have observed the full derivative spectrum. From the temperature dependence and extremum of dX''/dB, it is clear that these signals are from transitions between the $|\pm 1'\rangle$ states. For finite transition probability ($\sim |\langle +1'|S_z|-1'\rangle|^2$), we must have $E \neq 0$. Reasonable simulations of the absorption spectra are obtained with $E_0/k = 0.06$ K and $\sigma_E/k = 0.06$ K (σ_E is one standard deviation from the center value E_0) as shown in Figs. 2b and 2c. Thus, about 40% of the molecules have zero-field splittings which exceed $h\nu$. It is plausible that the difference between spectra and simulations is due to deviation from the assumed Gaussian distribution in E.

Figure 3 shows dX''/dB of polycrystalline (Zn/Fe)FS. Simulation of this spectrum using the single crystal parameter set gives a reasonable fit. However, the temperature dependence of this signal is different than that for the single crystal. The single crystal signal peaks at ~15 K [$D/k = 20.6$ K (*13*)] whereas the polycrystal signal does not. Further work is needed to determine the temperature dependence of the polycrystal signal more accurately.

Aqueous ferrous sulfate is an easily prepared sample and is useful as a reference to frozen solution data. EPR and magnetic susceptibility results are shown in Figs. 4 and 5. The positions of the valleys in Fig. 4 suggest that the signals are due to resonance

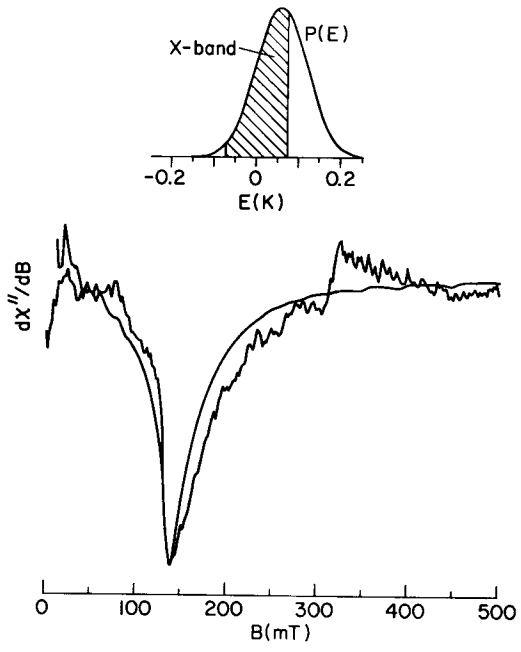

FIG. 3. Polycrystal EPR spectrum and simulation of (Zn/Fe)FS at $T \approx 15$ K using $B_1 \parallel B$. The simulation uses the zero-field parameters given in Fig. 2. The zero-field parameter distribution is shown above; the shaded region is the range of E observable at X band. Instrumental parameters: microwave, 9.127 GHz at 0.2 mW; modulation, 100 kHz at 0.8 mT_{pp}; gain, 4×10^6; field sweep, 3.5 mT/s; eight scans in 27 min.

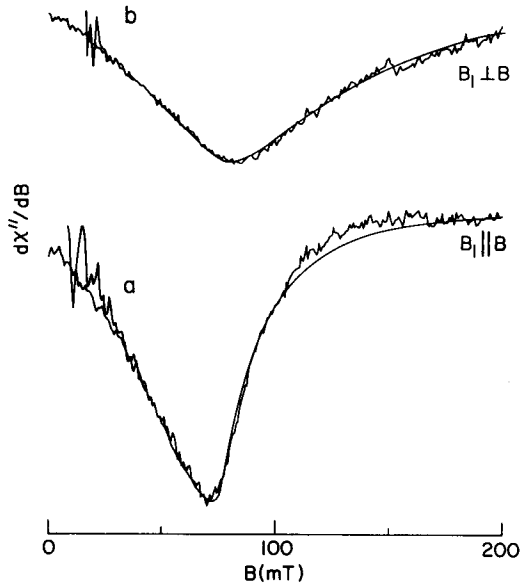

FIG. 4. EPR spectra and simulations of a frozen solution of 10 mM $FeSO_4$ at $T = 4$ K using (a) $B_1 \parallel B$ and (b) $B_1 \perp B$. Simulation parameters: $D/k = -10$ K, $E_0/k = 1.7$ K, $\sigma_E/k = 0.45$ K, $\mathbf{g}_0 = (2.00, 2.05, 2.16)$. $\mathbf{g}_0$ represents the g tensor values calculated with Eq. [2] using the central zero-field parameter; 15% of the molecules have zero-field energy splittings less than $h\nu$. Instrumental parameters: microwave (a) 9.064 GHz or (b) 8.993 GHz at 2 mW; modulation 100 kHz at 0.8 mT_{pp}; gain, 10^6; field sweep, 1 mT/s.

from the $|\pm 2'\rangle$ states. Simulation of the magnetic susceptibility data gives $D/k = \pm 13$ K and $E/D \approx 1/3$, while the best simulation of the EPR spectra is obtained with $D/k = -10$ K, $E_0/k = 1.7$ K, and $\sigma_E/k = 0.45$ K. Also shown in Fig. 4 is a spectrum

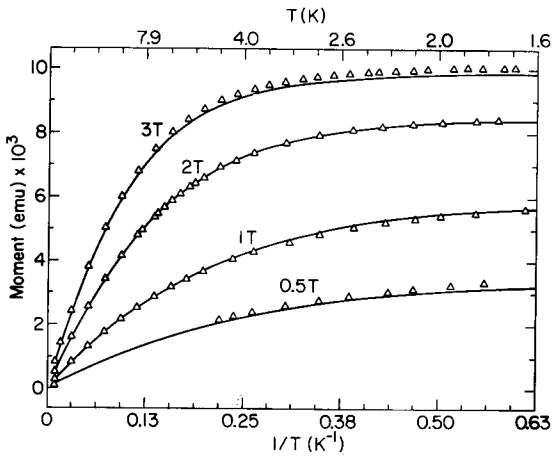

FIG. 5. Magnetic susceptibility measurements and simulation of a frozen solution of 13 mM $FeSO_4$ in D_2O at various magnetic fields. Simulation parameters: $D/k = 13$ K, $E/k = 3.4$ K, 0.77 μmol of iron, $\mathbf{g} = (2.13, 2.23, 2.00)$. The susceptometer was a SQUID S.H.E. VTS-50.

taken in the $B_1 \perp B$ mode and a simulation using the same parameters. From the temperature dependence of the EPR signal, we conclude that the signal arises from a ground state doublet, which is in agreement with the simulation. A clue to this can also be found in noting the position of the valley in Fig. 3; it is at a slightly lower field compared to similar features from compounds having positive D values. The shift in field results from $g_{zz} > 2$ (Eq. [2], $D < 0$). We point out that our D value, both in sign and in magnitude, contradicts Hagen's (*7*) interpretation of the EPR spectra. We have also performed similar experiments on frozen solutions of Fe^{2+}EDTA and find from magnetic susceptibility measurements $D/k = \pm 13$ K, $E/D = 1/3$, again in contradiction with Hagen's interpretation. The FeEDTA EPR spectrum is quite different from that of Fig. 4a, but the temperature dependence suggests $D/k \approx -15$ K. We point out that the signal is quite similar to that of the deoxyhemerythrin azide complex. It has been suggested that the EPR signal of the deoxyhemerythrin azide complex arises from a binuclear iron center with a weak exchange coupling (*15*). Evidence exists for dimeric ferric forms of iron EDTA (*16*); thus perhaps the FeEDTA EPR signal is due to a binuclear center.

Figure 6 shows the first EPR spectra reported from quintet states of myoglobin. These spectra are seen only under optimal conditions: low temperature, high gain,

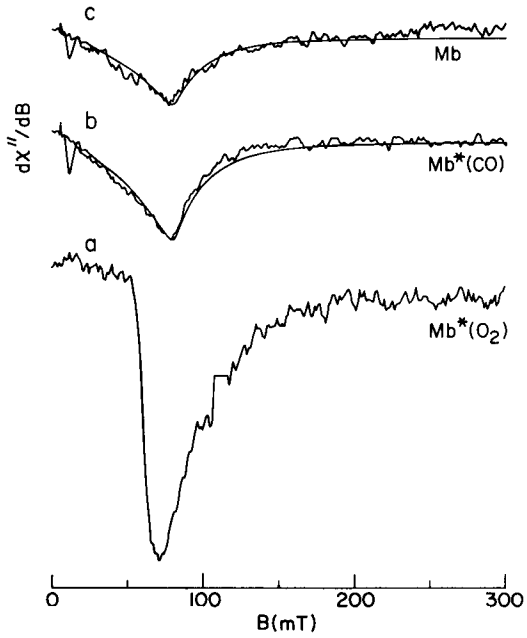

FIG. 6. Frozen solution EPR spectra and simulation of (a) photolyzed oxymyoglobin, Mb*(O_2); (b) photolyzed carbonmonoxymyoglobin, Mb*(CO); and (c) deoxymyoglobin, Mb, all at $T = 4$ K using $B_1 \parallel B$. All samples are 10 mM myoglobin, 50 mM KP_i, pH = 7. The simulations of Mb and Mb*(CO) are identical except for the vertical scale. Simulation parameters: $D_0/k = 7$ K, $\sigma_D/k = 1.5$ K, $E_0/k = 1$ K, $\sigma_E/k = 0.25$ K, $\mathbf{g}_0 = (2.07, 2.09, 2.00)$. Instrumental parameters: microwave, 9.1 GHz at 2 mW; modulation, 100 kHz at 0.8 mT_{pp}; gain, 1.6×10^6; field sweep, 1.5 mT/s; five scans in 17 min. There is a subtraction artifact at $B = 120$ mT in (a).

high power, and signal averaging. Difference spectra between the diamagnetic CO-adduct of Mb and its photolysis product Mb*(CO) are virtually identical with the spectra of deoxyMb, whereas the difference spectra of the O_2 complex and its photoproduct Mb*(O_2) are markedly dissimilar. Though somewhat weaker, the Mb and Mb*(CO) spectra have approximately the same shape as that of Fig. 4a, but the valley is at a slightly higher field. The Mb*(CO) and Mb*(O_2) signals disappear upon warming of the samples to 100 K for 10 min to allow for recombination and can be reproducibly cycled in this manner. This allows light minus dark subtractions, which are necessary to determine the proper signal shape. The positions of the valleys in Fig. 6 suggest that the signals are due to resonance from the $|\pm 2'\rangle$ states. Simulations of the Mb and Mb*(CO) spectra are compatible with magnetic susceptibility (*17*) and far-infrared (*4*) results if one assumes a large spread in D as well as E values. Parameters used in the simulations in Fig. 6 are $D_0/k = 7$ K, $\sigma_D/k = 1.5$ K, $E_0/k = 1$ K, and $\sigma_E/k = 0.25$ K. We have also simulated the Mb*(CO) magnetic susceptibility data of Roder *et al.* (*17*) with and without zero-field distributions comparable in width to those of the EPR simulations: no significant difference was found. This is not surprising since magnetic susceptibility measures the bulk moment.

From the temperature dependence of the deoxyMb spectrum in Fig. 7, we conclude that the signal is from an excited doublet ($D > 0$). Quantitative information is difficult to obtain as above 10 K lineshape changes cause a rapid decrease in dX''/dB. The signal is no longer visible at ~25 K. In sharp contrast are spectra of the frozen solutions of $FeSO_4$ and FeEDTA, where no lineshape change is observed up to at least 50 K for FeEDTA. A possible explanation is a faster spin relaxation in the excited doublet of the Mb complexes relative to that for a ground doublet in the frozen solution of $FeSO_4$. The latter signal saturates at a lower microwave power in agreement with this explanation. The validity of the spin Hamiltonian for Mb has been questioned (*4, 18, 19*), as possible nearby orbital states may be populated at higher temperatures. Since the EPR signals presented here for Mb are seen only at low temperatures, the question of validity can not be addressed with our data.

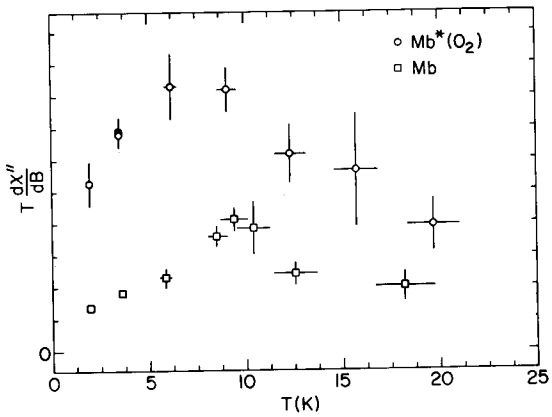

FIG. 7. Temperature dependence of the EPR signals in Fig. 6 for Mb (□) and Mb*(O_2) (○). Signal intensity is determined from the depth of the valley at 70 mT. Reproducible signal intensity at 3.5 K for Mb*(O_2) after measurements at 15.7 and 19.7 K confirms the lack of recombination during the experiment.

A particularly interesting spectrum is found from Mb*(O_2), shown in Fig. 6a. The shape and intensity are quite different from those of the deoxyMb, Mb*(CO), and hexaquo iron (Fig. 4a) spectra. The signal is relatively large in view of Mössbauer evidence that suggests only 30% of the molecules contribute. The temperature dependence in Fig. 7 is similar to the deoxyMb data implying that the signal is from an excited doublet; however, the spectrum (Fig. 6a) cannot be simulated with our model. In the case of Mb*(O_2), the drop in dX''/dB above 8 K was not due to recombination as the full signal was recovered at 3.4 K after taking data at higher temperatures. A possible reason for the spectral differences may be magnetic coupling of the spin $S = 2$ iron and the spin $S = 1$ O_2. The spectra may thus contain information about the position of the O_2 molecule relative to the heme iron. We are currently working on this problem.

Figure 8 shows polycrystal EPR spectra of the model heme complex Fe(II) 2-methylimidazole mesotetraphenylporphyrin (FeTPP) (*20*) in both the $B_1 \perp B$ and $B_1 \parallel B$ modes. FeTPP is a sterically hindered 5-coordinate d^6 complex. The spectra are similar to those of Fig. 4 and show a slight shift to lower field relative to those of the deoxyMb and Mb*(CO) complexes. Thus, the FeTPP signal is due to resonance from the $|\pm 2'\rangle$ states. The EPR simulations use $D/k = -16$ K, $E_0/k = 1.7$ K, and $\sigma_E/k = 0.45$ K, values that differ sizably from those used in the interpretation of the Mössbauer measurements (*21*) of $D/k = -7.6$ K and $E/k = -3.9$ K.

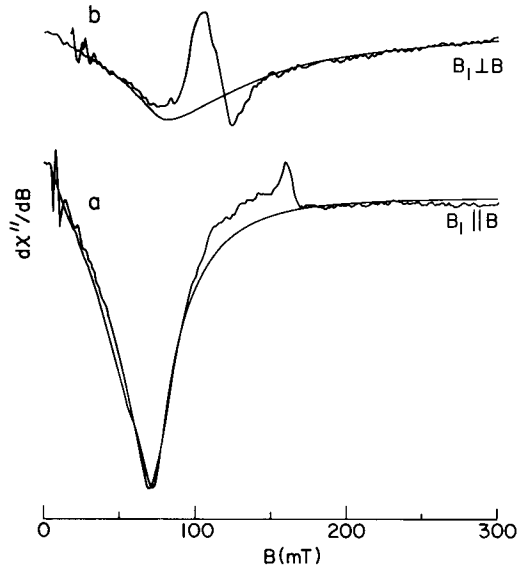

FIG. 8. Polycrystal EPR spectra and simulations of Fe(II) 2-methylimidazole mesotetraphenylporphyrin at $T = 4$ K using (a) $B_1 \parallel B$ and (b) $B_1 \perp B$. The signal at 140 mT in (a) and 110 mT in (b) is a ferric impurity. Simulation parameters: $D/k = -16$ K, $E_0/k = 1.7$ K, $\sigma_E/k = 0.45$ K, $g_0 = (2.00, 2.04, 2.20)$. Thirty-five percent of the molecules have zero-field energy splittings less than $h\nu$. Instrumental parameters: microwave (a) 9.073 GHz or (b) 8.999 GHz at 0.2 mW; modulation, 100 kHz at 0.8 mT_{pp}; gain, 8×10^5; field sweep, 1.5 mT/s.

In conclusion, we have discovered EPR signals from a "benchmark" protein and we provide a basis for the analysis of these signals and those of other integer spin complexes. These spectra and analyses may eventually lead to a better understanding of the Mb active center and provide a reference for experiments using higher spectrometer energies.

ACKNOWLEDGMENTS

We are indebted to Dr. Gerald Wagner for help in the sample preparation and to Dr. Christopher Reed for supplying the model heme complex. We gratefully acknowledge the support of the Illinois ESR Center. This work was funded in part by NIH Grant GM16406.

REFERENCES

1. M. P. HENDRICH, G. C. WAGNER, AND P. G. DEBRUNNER, *Bull. Am. Phys. Soc.* **32,** 479 (1987).
2. A. ABRAGAM AND B. BLEANEY, "Electron Paramagnetic Resonance of Transition Ions," Chap. 3, Clarendon Press, Oxford, 1970.
3. P. M. CHAMPION AND A. J. SIEVERS, *J. Chem. Phys.* **66,** 1819 (1977).
4. P. M. CHAMPION AND A. J. SIEVERS, *J. Chem. Phys.* **72,** 1569 (1980).
5. R. S. RUBINS AND H. R. FETTERMAN, *J. Chem. Phys.* **71,** 5163 (1979).
6. P. LEVIN, Ph.D. thesis, University of Virginia (1984).
7. W. R. HAGEN, *Biochim. Biophys. Acta* **708,** 82 (1982).
8. J. M. BAKER AND B. BLEANEY, *Proc. R. Soc. London, Ser. A* **245,** 156 (1958).
9. R. AASA AND T. VÄNNGÅRD, *J. Magn. Reson.* **19,** 308 (1975).
10. R. ZIMMERMANN, H. SPIERING, AND G. RITTER, *Chem. Phys.* **4,** 133 (1974).
11. G. C. BRACKETT, P. L. RICHARDS, AND W. S. CAUGHEY, *J. Chem. Phys.* **54,** 4383 (1971).
12. R. S. RUBINS, *Proc. Phys. Soc. London* **80,** 244 (1962).
13. F. VARRET, *J. Phys. Chem. Solids* **37,** 257 (1976).
14. C. E. JOHNSON, *Proc. Phys. Soc. London* **92,** 748 (1967).
15. R. C. REEM AND E. I. SOLOMON, *J. Am. Chem. Soc.* **109,** 1216 (1987).
16. S. J. LIPPARD, H. SCHUGAR, AND C. WALLING, *Inorg. Chem.* **6,** 1825 (1967).
17. H. RODER, J. BERENDZEN, S. F. BOWNE, H. FRAUENFELDER, T. B. SAUKE, E. SHYAMSUNDER, AND M. B. WEISSMAN, *Proc. Natl. Acad. Sci. USA* **81,** 2359 (1984).
18. Y. ALPERT, Ph.D. thesis, University of Paris (1975).
19. T. A. KENT, K. SPARTALIAN, AND G. LANG, *J. Chem. Phys.* **71,** 4899 (1979).
20. J. P. COLLMAN AND C. A. REED, *J. Am. Chem. Soc.* **95,** 2048 (1973).
21. T. A. KENT, K. SPARTALIAN, G. LANG, T. YONETONI, C. A. REED, AND J. P. COLLMAN, *Biochim. Biophys. Acta* **580,** 245 (1979).